Electronic Supplementary Material (ESI) for Inorganic Chemistry Frontiers.


# Supporting Information: Nanoscale chemical speciation of β-amyloid/iron aggregates using soft x-ray spectromicroscopy

James Everett, *[ab] Jake Brooks, [b] Joanna F. Collingwood [b] and Neil D. Telling [a]

[a] *School of Pharmacy and Bioengineering, Guy Hilton Research Centre, Thornburrow Drive, Keele University, Staffordshire, ST4 7QB, UK. E-mail: j.everett@keele.ac.uk*

[b] *School of Engineering, Library Road, University of Warwick, Coventry, CV4 7AL, UK.*

## Table of Contents

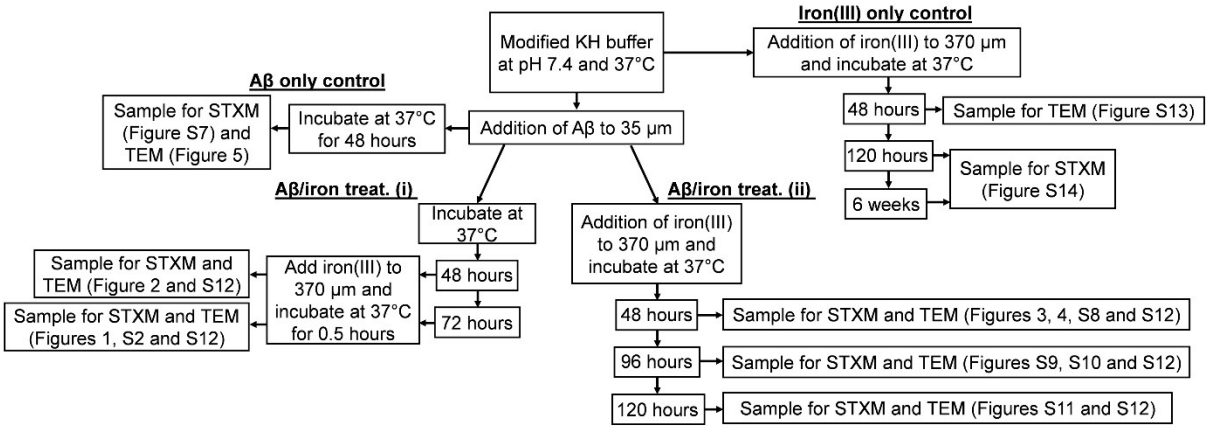


**Figure S1.** A flow chart summarizing the preparation methods used for each sample type in this study.

## Results

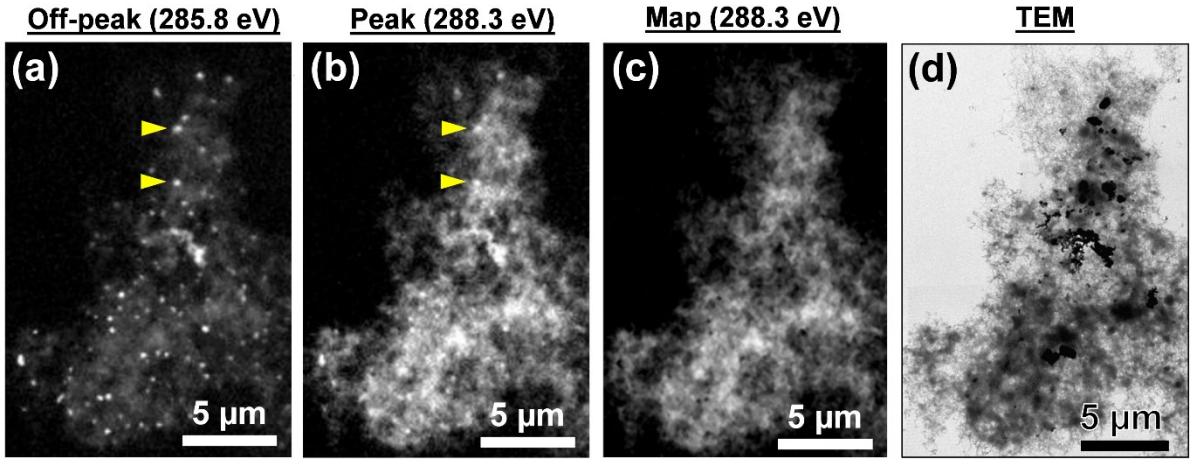


**Figure S2.** The process of STXM speciation mapping (at the carbon *K*-edge) and a TEM image of the aggregate shown in Figure 1 of the main text. **(a)** Single energy off-peak image taken at 286.8 eV. **(b)** Peak image taken at 288.3 eV. Both (a) and (b) display artefacts (bright spots) from the drying process, examples of which are highlighted with yellow arrowheads. **(c)** Artefact-free carbon *K*-edge speciation map showing peptide content, created by subtracting (a) from (b). **(d)** TEM image.

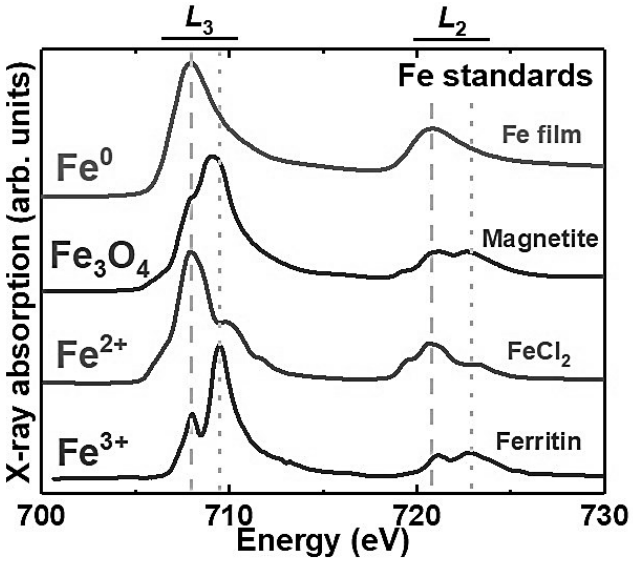


**Figure S3.** Reference iron $L_{2,3}$-edge x-ray absorption spectra from four iron standards. Dashed and dotted lines show the principal energy positions for $Fe^{2+}/Fe^{0}$ and $Fe^{3+}$ absorption peaks respectively.

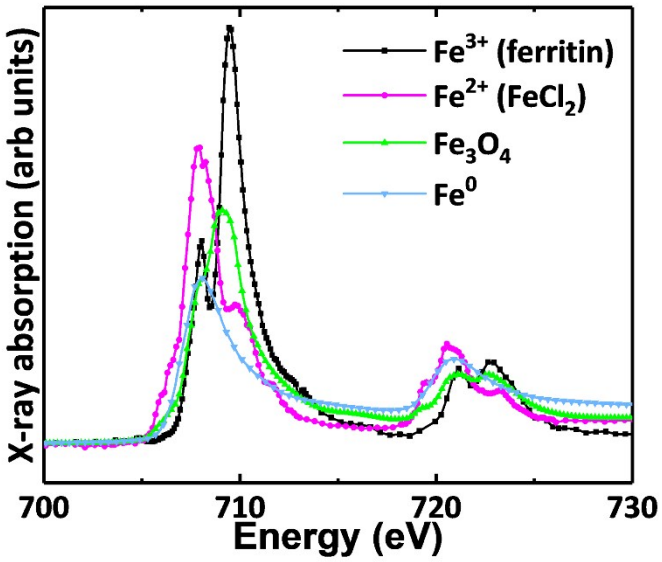


**Figure S4.** Scaled iron $L_{2,3}$-edge x-ray absorption reference spectra used to fit experimental iron spectra. Originally presented in [1].

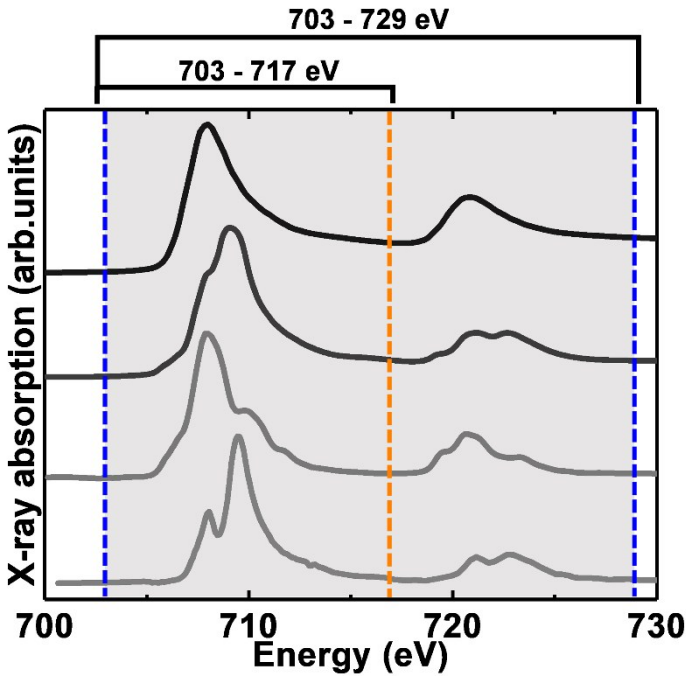


**Figure S5.** The energy ranges used for fitting of the experimental iron $L_{2,3}$-edge x-ray absorption spectra. See also Table S1.

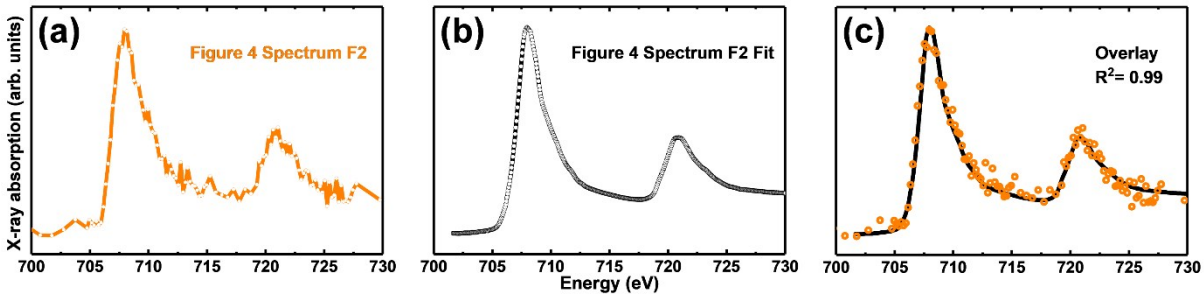


**Figure S6.** An example overlay plot created from the fitting of an experimental iron $L_{2,3}$-edge x-ray absorption spectrum. **(a)** Experimental spectrum, **(b)** corresponding fit, **(c)** overlay showing experimental data (coloured circles) and fit (black line). An $R^2$ value describing the strength of correlation between the fit and the experimental spectrum is also provided.

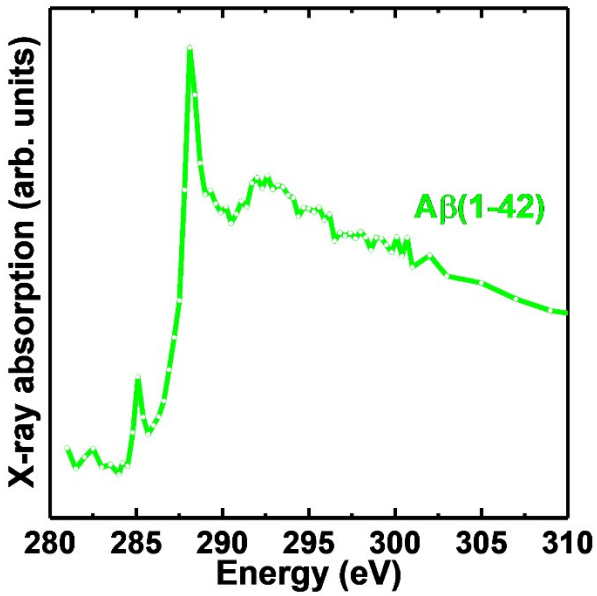


**Figure S7.** Carbon *K*-edge x-ray absorption spectrum from Aβ(1-42) in KH buffer.

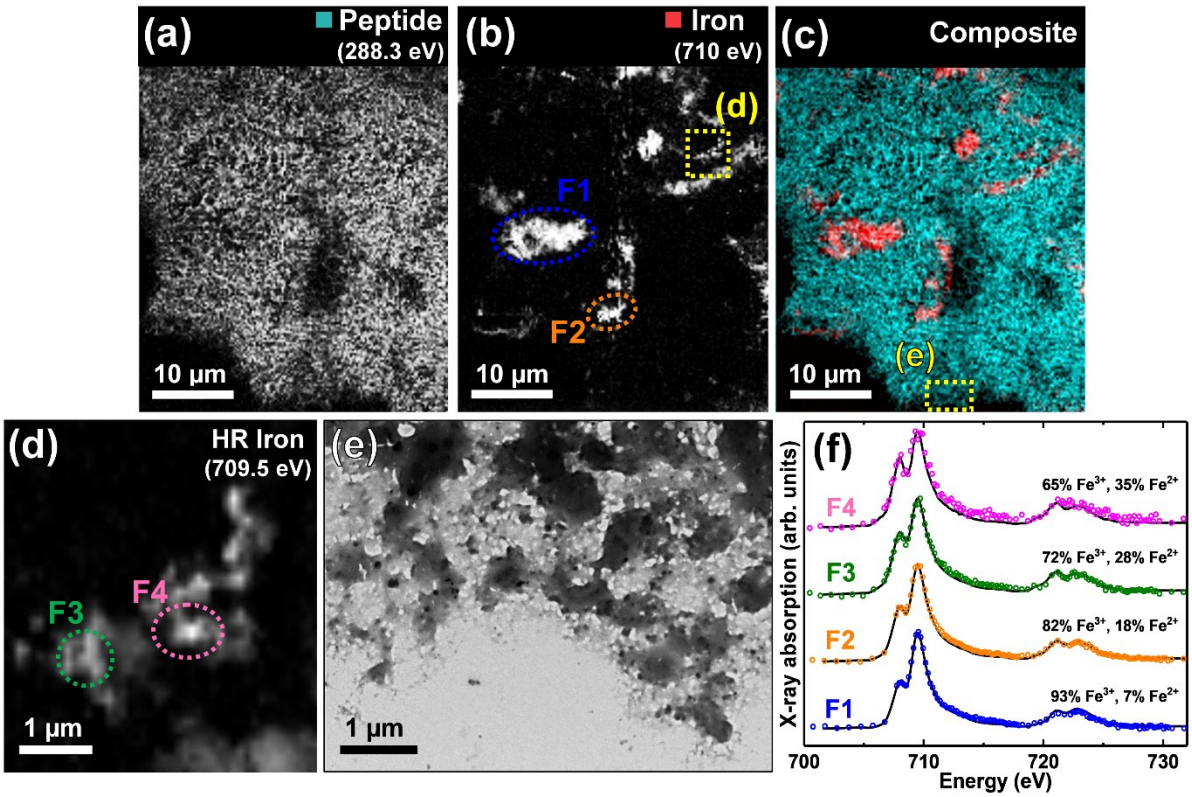


**Figure S8**. STXM speciation maps, TEM image and iron $L_{2,3}$-edge x-ray absorption spectra from a Aβ/iron aggregate formed following 48 hours of Aβ/iron co-incubation. **(a)** Carbon *K*-edge peptide map. **(b)** Iron $L_3$-edge map. **(c)** Composite image showing peptide (cyan) and iron (red) content. **(d)** High-resolution iron $L_3$-edge map of the yellow highlighted region in (b). **(e)** TEM image of the region highlighted in (c). **(f)** Iron $L_{2,3}$-edge x-ray absorption spectra from the regions highlighted in (b) and (d). The solid lines for the spectra correspond to best fit curves created by superposition of suitably scaled iron reference x-ray absorption spectra.

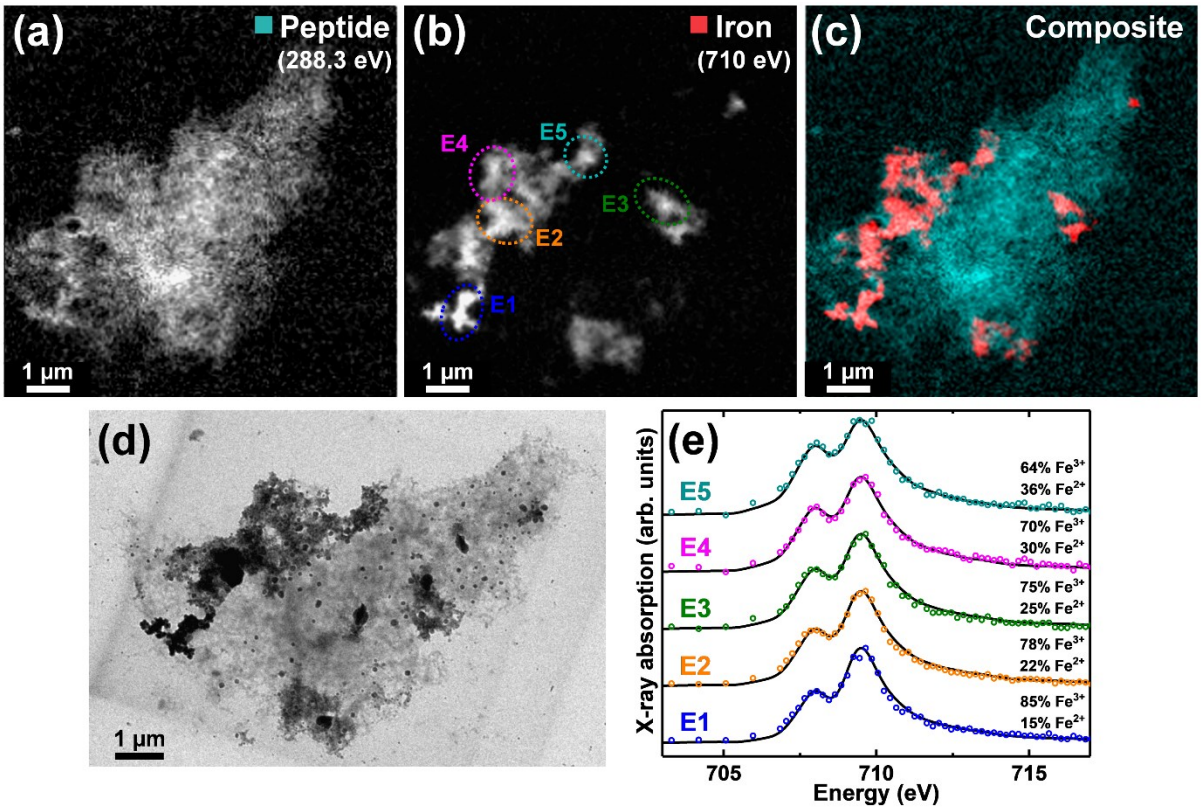


**Figure S9**. STXM speciation maps, TEM image and iron $L_3$-edge x-ray absorption spectra from a Aβ/iron aggregate formed following 96 hours of Aβ/iron co-incubation. **(a)** Carbon *K*-edge peptide map. **(b)** Iron $L_3$-edge map. **(c)** Composite image showing peptide (cyan) and iron (red) content. **(d)** TEM image. **(e)** Iron $L_3$-edge x-ray absorption spectra from the regions highlighted in (b). The solid lines for the spectra correspond to best fit curves created by superposition of suitably scaled iron reference x-ray absorption spectra. Panels (a)-(d) originally presented in [2].

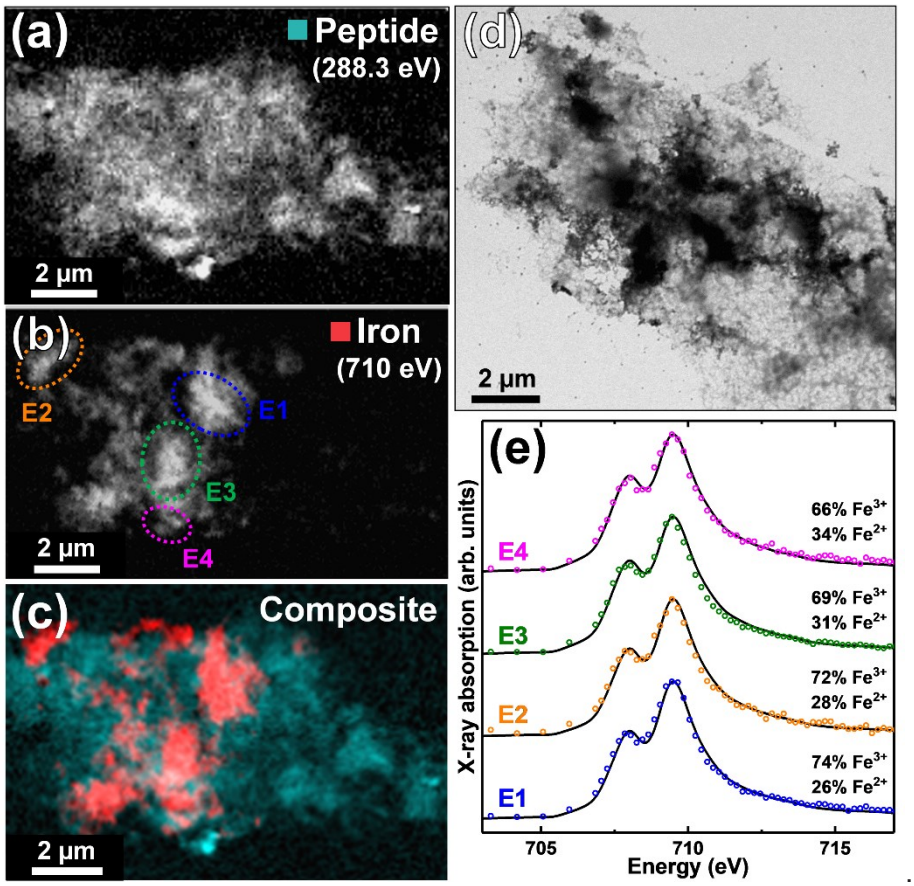


**Figure S10**. STXM speciation maps, TEM image and iron $L_3$-edge x-ray absorption spectra from a Aβ/iron aggregate formed following 96 hours of Aβ/iron co-incubation. **(a)** Carbon *K*-edge peptide map. **(b)** Iron $L_3$-edge map. **(c)** Composite image showing peptide (cyan) and iron (red) content. **(d)** TEM image. **(e)** Iron $L_3$-edge x-ray absorption spectra from the regions highlighted in (b). The solid lines for the spectra correspond to best fit curves created by superposition of suitably scaled iron reference x-ray absorption spectra. Panels (a)-(c) originally presented in [2].

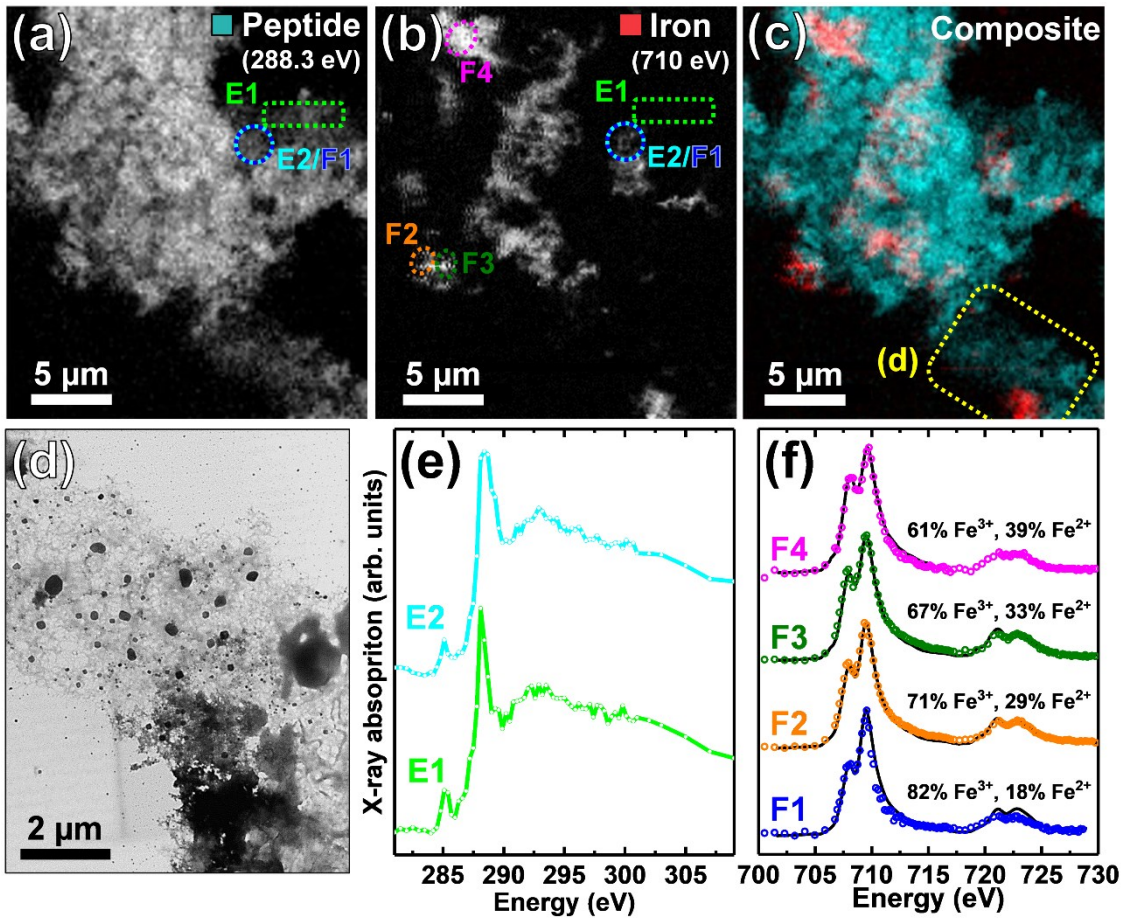


**Figure S11.** STXM speciation maps, TEM image carbon *K*-edge x-ray absorption spectra and iron $L_{2,3}$-edge x-ray absorption spectra from a Aβ/iron aggregate formed following 120 hours of Aβ/iron co-incubation. **(a)** Carbon *K*-edge peptide map. **(b)** Iron $L_3$-edge map. **(c)** Composite image showing peptide (cyan) and iron (red) content. **(d)** TEM image. **(e)** Carbon *K*-edge x-ray absorption spectra from the regions highlighted in (a) and (b). **(f)** Iron $L_{2,3}$-edge x-ray absorption spectra from the regions highlighted in (a) and (b). The solid lines for the spectra correspond to best fit curves created by superposition of suitably scaled iron reference x-ray absorption spectra.

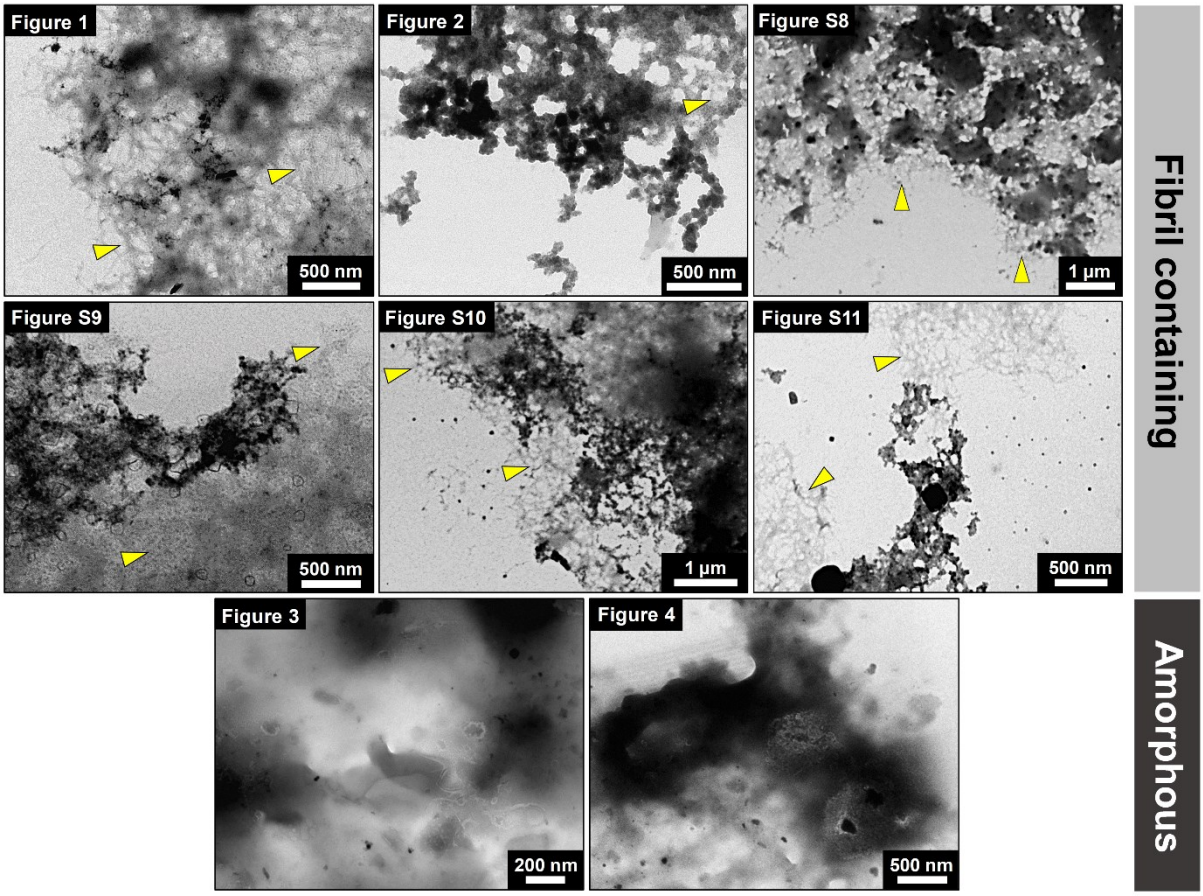


**Figure S12.** TEM images from all Aβ/iron aggregates displayed in this manuscript. Aggregates are categorised according to their fibril containing (top) or amorphous (bottom) morphology. Example regions of fibrillar Aβ are highlighted by yellow arrowheads. Variations in the appearance and definition of fibrils within the fibril containing aggregates were apparent upon iron loading, and as a result of density changes within the aggregate structures.

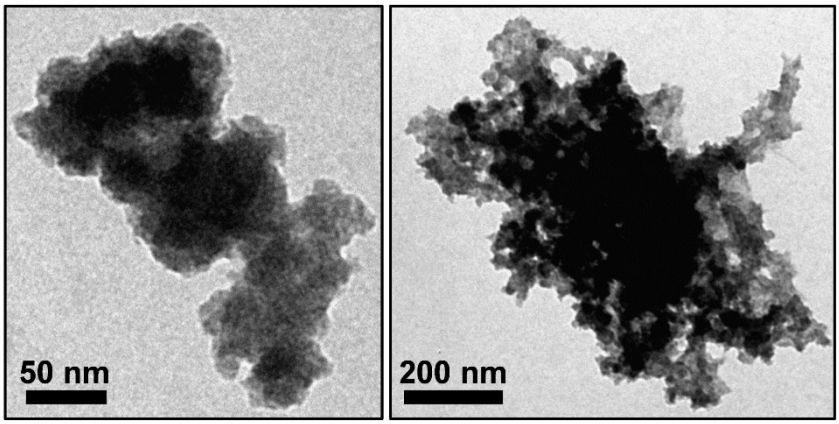


**Figure S13**. TEM images showing insoluble iron precipitates formed following the addition of iron(III) to the KH buffer.

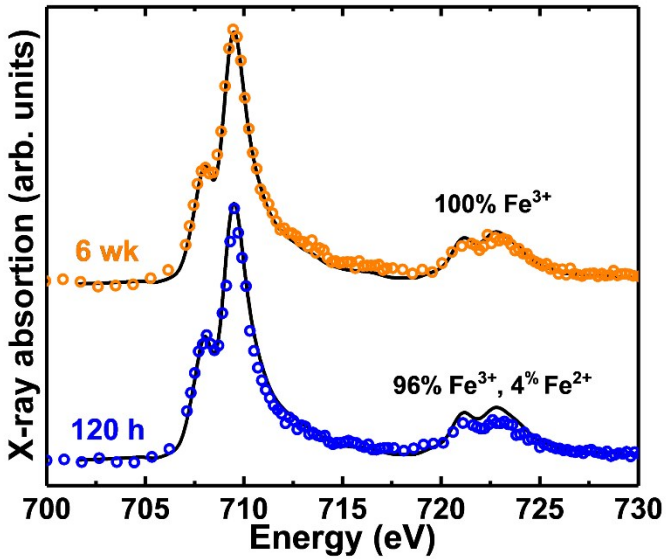


**Figure S14.** Iron $L_{2,3}$-edge x-ray absorption spectrum from iron(III) incubated in KH buffer. Incubation time indicated to the left of each spectrum. The solid lines for the spectra correspond to best fit curves created by superposition of suitably scaled iron reference x-ray absorption spectra.

**Table S1.** Fitting values and parameters for the displayed experimental iron $L_{2,3}$-edge x-ray absorption spectra. Fitting was limited to the $L_3$-edge only (703-717eV) for the iron spectra shown in Figures S9, S10 and S11 F4 to avoid fitting excessively noisy and distorted parts of the experimental spectrum that were apparent at the iron $L_2$-edge.

| Spectrum | Calculated Fit | $R^2$ Value | Fitting Region (eV) |
|---|---|---|---|
| Figure 1 F1 | 88% $Fe^{3+}$, 12% $Fe^{2+}$ | 0.98 | 703-729 |
| Figure 1 F2 | 86% $Fe^{3+}$, 14% $Fe^{2+}$ | 0.98 | 703-729 |
| Figure 1 F3 | 72% $Fe^{3+}$, 28% $Fe^{2+}$ | 0.96 | 703-729 |
| Figure 2 F1 | 85% $Fe^{3+}$, 15% $Fe^{2+}$ | 0.97 | 703-729 |
| Figure 2F2 | 81% $Fe^{3+}$, 19% $Fe^{2+}$ | 0.99 | 703-729 |
| Figure 2 F3 | 81% $Fe^{3+}$, 19% $Fe^{2+}$ | 0.98 | 703-729 |
| Figure 2 F4 | 80% $Fe^{3+}$, 20% $Fe^{2+}$ | 0.97 | 703-729 |
| Figure 3 F1 | 100% $Fe^{3+}$ | 0.96 | 703-729 |
| Figure 3 F2 | 78% $Fe^{3+}$, 22% $Fe^{2+}$ | 0.96 | 703-729 |
| Figure 3 F3 | 80% $Fe_3O_4$, 20% $Fe^{3+}$ | 0.96 | 703-729 |
| Figure 3 F4 | 55% $Fe^{0}$, 33% $Fe^{3+}$, 12% $Fe^{2+}$ | 0.98 | 703-729 |
| Figure 4 F1 | 100% $Fe^{3+}$ | 0.85 | 703-729 |
| Figure 4 F2 | 85% $Fe^{0}$, 15% $Fe^{2+}$ | 0.99 | 703-729 |
| Figure S8 F1 | 93% $Fe^{3+}$, 7% $Fe^{2+}$ | 0.98 | 703-729 |
| Figure S8 F2 | 82% $Fe^{3+}$, 18% $Fe^{2+}$ | 0.99 | 703-729 |
| Figure S8 F3 | 72% $Fe^{3+}$, 28% $Fe^{2+}$ | 0.97 | 703-729 |
| Figure S8 F4 | 65% $Fe^{3+}$, 35% $Fe^{2+}$ | 0.92 | 703-729 |
| Figure S9 E1 | 85% $Fe^{3+}$, 15% $Fe^{2+}$ | 0.99 | 703-717 |
| Figure S9 E2 | 78% $Fe^{3+}$, 22% $Fe^{2+}$ | 0.99 | 703-717 |
| Figure S9 E3 | 75% $Fe^{3+}$, 25% $Fe^{2+}$ | 0.99 | 703-717 |
| Figure S9 E4 | 70% $Fe^{3+}$, 30% $Fe^{2+}$ | 0.99 | 703-717 |
| Figure S9 E5 | 64% $Fe^{3+}$, 36% $Fe^{2+}$ | 0.99 | 703-717 |
| Figure S10 E1 | 74% $Fe^{3+}$, 26% $Fe^{2+}$ | 0.99 | 703-717 |
| Figure S10 E2 | 72% $Fe^{3+}$, 28% $Fe^{2+}$ | 0.99 | 703-717 |
| Figure S10 E3 | 69% $Fe^{3+}$, 31% $Fe^{2+}$ | 0.99 | 703-717 |
| Figure S10 E4 | 66% $Fe^{3+}$, 34% $Fe^{2+}$ | 0.99 | 703-717 |
| Figure S11 F1 | 82% $Fe^{3+}$, 18% $Fe^{2+}$ | 0.96 | 703-728 |
| Figure S11 F2 | 71% $Fe^{3+}$, 29% $Fe^{2+}$ | 0.99 | 703-729 |
| Figure S11 F3 | 67% $Fe^{3+}$, 33% $Fe^{2+}$ | 0.99 | 703-729 |
| Figure S11 F4 | 61% $Fe^{3+}$, 39% $Fe^{2+}$ | 0.99 | 703-717 |
| Figure S14 120 h | 96% $Fe^{3+}$, 4% $Fe^{2+}$ | 0.98 | 703-729 |
| Figure S14 6 wk | 100% $Fe^{3+}$ | 0.98 | 703-729 |

## References


1. J. Everett, J. F. Collingwood, V. Tjendana-Tjhin, J. Brooks, F. Lermyte, G. Plascencia-Villa, I. Hands-Portman, J. Dobson, G. Perry and N. D. Telling, Nanoscale synchrotron X-ray speciation of iron and calcium compounds in amyloid plaque cores from Alzheimer's disease subjects, *Nanoscale*, 2018, **10**, 11782-11796.
2. J. Everett, E. Cespedes, L. R. Shelford, C. Exley, J. F. Collingwood, J. Dobson, G. van der Laan, C. A. Jenkins, E. Arenholz and N. D. Telling, Ferrous iron formation following the co-aggregation of ferric iron and the Alzheimer's disease peptide beta-amyloid (1-42), *Journal of the Royal Society Interface*, 2014, **11**.